HADLEY CENTRE TECHNICAL NOTE NO. 5

AN ANALOGUE MODEL TO DERIVE ADDITIONAL CLIMATE CHANGE SCENARIOS FROM EXISTING GCM SIMULATIONS

by

C.Huntingford and P.M. Cox

Submitted to Climate Dynamics

January 1999

Hadley Centre for Climate Prediction and Research
Meteorological Office
London Road
Bracknell
Berkshire RG12 2SY

An analogue model to derive additional climate change scenarios from existing GCM simulations

[1]C. Huntingford and [2]P. M. Cox

[1]Institute of Hydrology, Wallingford, Oxon, OX10 8BB, UK
[2]Hadley Centre, Met Office, Bracknell, Berks, RG12 2SY, UK

January 26, 1999

Abstract

Changes in land surface driving variables, predicted by GCM transient climate change experiments and as required for impact studies, are demonstrated to exhibit linearity in the global mean land temperature anomaly, ΔT_l. The associated constants of proportionality retain the spatial and seasonal characteristics of the GCM output, whilst ΔT_l can be directly related to radiative forcing anomalies. The resultant analogue model is shown to be robust between GCM runs and as such provides a computationally efficient technique of extending existing GCM experiments to a large range of climate change scenarios.

1 Introduction

There is currently worldwide interest in the impact of fossil fuel emissions upon climate. Of particular concern is the accumulation of extra atmospheric greenhouse gases (most notably CO_2), which increases the absorption of outgoing longwave radiation. The atmosphere and oceans respond to this extra radiative forcing by an increase in global temperature as the climate strives to meet a new radiative equilibrium. Global Circulation Models (GCMs) are numerical models that provide a quantitative assessment of such warming effects. All important climate processes and their internal feedback mechanisms and couplings must be explicitly modelled within the GCM, complete with appropriate parameterisations. Internal model variability should be able to replicate the observed climatic variations that occur on a range of timescales.

Important GCM diagnostics are predicted changes in land surface climatology as a consequence of a change in radiative forcing. This includes quantities such as surface temperature, rainfall rate and downward radiation, all of which affect the behaviour of the land surface. These diagnostics may be used to drive hydrological and ecological impacts models. Such an off-line analysis provides valuable information as to possible modes of behaviour of the system of interest. Further, such analysis may also provide guidance to the relative importance of different land surface parameterisations and therefore direct the development of field experiments. However, there are difficulties associated with this modelling process. Due to the large computational requirement of GCMs, only a limited number of long term simulations may be made. It is conceivable that some potential land surface responses will not be observed for the existing anthropogenic emission scenarios prescribed to the GCM. Conversely, it is potentially difficult to determine whether observed terrestrial model behaviours are generic or a consequence of the particular scenario chosen.

A methodology is required that can interpolate land surface anomalies from existing GCM transient runs to those appropriate to a range of greenhouse gas emission scenarios. For this purpose, a model is developed which operates as an analogue to the GCM. This model generates, with minimal computational requirement, and for prescribed radiative forcing, changes in land surface climatology. This analogue model is based upon the hypothesis that to a high degree of accuracy, GCM generated anomalies on the decadal timescale may be represented as the global mean land temperature multiplied by a spatial pattern. That is, temporal and spatial anomaly behaviours are amenable to separation of variables. The spatial pattern is unique to each climate variable, and there is already some evidence that such a decoupling of long-term temporal behaviour from geographical variability is valid (see Mitchell et al. (1998) for analysis of temperature fields)

2 The development and calibration of a GCM Analogue Model

2.1 Analogue model structure

It is hypothesised that GCM predictions of changes (or anomalies) in land surface climatology, at the decadal timescale and for a prescribed estimate of anthropogenic perturbations of radiative forcing, can be replicated to acceptable accuracy by a simpler analogue model. This model assumes that the temporal and spatial behaviour of such anomalies may be separated into a persistent spatial pattern V_x (units dependent upon particular anomaly variable, V) multiplied by a time dependent function. The temporal component is related to increases in radiative forcing via the intermediate variable of global mean decadal temperature change (at 1.5 m and averaged across all land points and all months), ΔT_l (K). The form of the analogue model, for anomalies of a land surface variable V is therefore given by

$$\Delta V(i,j,k) = \Delta T_l(i) V_x(j,k). \tag{1}$$

Throughout this paper, Δ indicates anomalies relative to an assumed (pre-industrial) control climatology. Individual decades are indexed by integer i, months by j (thereby retaining seasonality) and land surface spatial position by k. There are 1631 land points corresponding to the GCM grid.

The separation of variables represented by Eq. 1 is carried out for nine surface and near surface variables: temperature at 1.5 m, ΔT (K), relative humidity at 1.5 m, Δr_h (%), zonal wind speed at 10.0 m, Δu (m s^{-1}), azimuthal windspeed at 10.0 m, Δv (m s^{-1}), downward longwave radiation, $\Delta R_{L\downarrow}$ (W m^{-2}), downward shortwave radiation, $\Delta R_{S\downarrow}$ (W m^{-2}), rainfall rate, ΔP_R (mm day^{-1}), snowfall rate, ΔP_S (mm day^{-1}) and surface pressure, Δp_0 (hPa). These anomalies are of importance (to varying degrees) for impact studies.

2.2 The transient GCM experiments

Anomalies in land surface climatology are extracted from Version 3 of the Hadley Centre coupled land-atmosphere-ocean GCM, "HadCM3" (Gordon et al. (1998)). The oceanic component of this model has 20 vertical levels and a relatively high horizontal resolution of 1.25° latitude by 1.25° longitude. This allows a much improved simulation of ocean heat transports, which is critically important in enabling HadCM3 to be used realistically for climate change simulations without requiring flux adjustments. The atmospheric component of HadCM3 retains a horizontal resolution of 2.5° latitude by 3.75° longitude and 19 atmospheric layers, but incorporates a number of new physics schemes (Pope et al. (Submitted)). Major changes from earlier model versions include a new radiation scheme (Edwards and Slingo (1996)), a parameterisation of momentum by convective processes (Kershaw and Gregory (1997)), and an improved land surface scheme that simulates the effects of soil water phase change and CO_2 induced stomatal closure (Cox et al. (1999)).

Anomalies are derived from three transient GCM experiments, each corresponding to different prescribed temporal profiles of increased radiative forcing ΔQ (W m^{-2}). These anomalies are used to provide calibration and verification of the effectiveness of the analogue model. All anomalies in land surface climatology are calculated relative to mean values derived from the long (equilibrium) control GCM run that precedes the transient GCM experiments. The control run uses a fixed CO_2 concentration of 290 ppmv.

The first model run corresponds to an extra radiative forcing appropriate to a cumulative increase in atmospheric CO_2, c_a (ppmv) by two percent per annum (Figure 1): this will be referred to as the 2% run. As there is a prescribed increase in atmospheric CO_2 only, ΔQ satisfies (Shine et al. (1990))

$$\Delta Q = 5.397 \ln \left[\frac{c_a(\tau)}{c_a(0)} \right] \tag{2}$$

where τ (yr) is the time from the beginning of the GCM simulation, and the model specific factor of 5.397 was diagnosed from short runs with HadCM3 (W.J. Ingram, personal communication). Hence for the 2% run, $\Delta Q = 5.397 \ln(1.02)\tau$, which corresponds to an increase in atmospheric CO_2 by a factor of 16.0 after 140 years. Such an extreme scenario is unrealistic but useful for analysing the GCM response to a rapidly increasing radiative forcing.

The second GCM experiment is identical to the 2% run for the first seventy years of model time, after which atmospheric CO_2 concentration is fixed, corresponding to $c_a(\tau) \approx 4c_a(0)$. This run will be referred to as the 4x run and is used within this paper to calibrate ΔT_l only.

The third model run corresponds to estimated historic greenhouse forcings between pre-industrial to present (1860 to 1990) due to increases of carbon dioxide, methane, nitrous oxide and CFC's followed by projected further increases of these gases in accordance with IPCC scenario IS92a (Houghton *et al.*, 1995). This GCM will be referred to as the GHG (GreenHouse Gas) run. The additional radiative forcings, ΔQ, are calculated as a composite of increases in the various greenhouse gases, although Eq. (2) may be inverted to provide effective CO_2 levels as if all other greenhouse gases are invariant. In the GHG run the effective CO_2 concentration increases by a factor of 3.2 from 1860 to 2100.

2.3 Global thermal behaviour: a model for ΔT_l

A simple global heat balance model is required to link the mean land temperature anomaly at the decadal timescale, ΔT_l, to the radiative forcing anomaly ΔQ. This submodel must contain sufficient physical realism for its internal parameters to be both well defined and robust to changes in the forcing scenario. The model developed below is calibrated against the 2% and 4x GCM runs, and then used predictively against the GHG GCM experiment.

2.3.1 Preliminary findings using a "one-box" heat balance model

Initially, a heat balance model comprising of a single component is considered. ΔT_l is assumed to satisfy $C^* \mathrm{d}\Delta T_l/\mathrm{d}t = \Delta Q(t) - \lambda \Delta T_l$ for areal heat capacity C^* (J K^{-1} m^{-2}), climate sensitivity λ (W m^{-2} K^{-1}) and time t (s). The thermal heat capacity is primarily associated with the oceans, and so this model must implicitly include any ocean-land advection. The optimum values of C^* and λ, found by least squares fitting against the 2% and GHG runs, are: $\lambda = 0.98$ W m^{-2} K^{-1}, $C^* = 3.3 \times 10^8$ J K^{-1} m^{-2} and $\lambda = 0.82$ W m^{-2} K^{-1}, $C^* = 9.2 \times 10^8$ J K^{-1} m^{-2} respectively. Analysis (not presented here) shows that a large range of (λ, C^*) pairs provide a good fit to each GCM run, and as such the selected optimal values cannot be regarded with confidence. Further, the range of good fit parameter pairs for the two GCM runs do not overlap and so the model is not robust between different forcing scenarios. On this basis, this single component model is rejected.

2.3.2 A "two-box" heat balance model

A model with separate components for the mean decadal land temperature anomalies and mean decadal ocean temperature anomalies, ΔT_o (K) is constructed. Although more complicated than the single-box model, additional diagnostics from the 2% and 4x GCM runs allow accurate evaluation of the new parameters. Extra GCM diagnostics (besides values of ΔT_l and ΔT_o) are anomalies in the decadal mean top of the atmosphere net downward radiation over land, $\Delta F_{TOA\downarrow,l}(t)$ (W m^{-2}) and over the ocean, $\Delta F_{TOA\downarrow,o}(t)$ (W m^{-2}). The global mean anomalies in top of the atmosphere net downward radiation, $\Delta F_{TOA\downarrow}$ satisfy $\Delta F_{TOA\downarrow} = f\Delta F_{TOA\downarrow,o} + (1-f)\Delta F_{TOA\downarrow,l}$ where $f = 0.711$ is the (gridbox) fraction of the Earth's surface covered by ocean. For an equilibrium climate, the absolute value of global mean top of the atmosphere radiative flux is approximately zero, although there may be a non-zero heat flux between the oceans and land.

Atmospheric radiative forcing due to changes in the concentration of atmospheric greenhouse gases, $\Delta Q(t)$, is assumed to be identical over both land and ocean. A downward heat flux into the oceans, ΔH_o (W m^{-2}), is included but the heat flux into the land is assumed to be negligible relative to other model terms (Murphy, 1995). The change in thermal advection between the two components is characterised by $\Delta H_a(t)$ (W m^{-2}), where for convenience this advective flux anomaly (per unit land area and defined positive towards the land) is expressed as $f\Delta H_a$. The heat budget equations, for all times, over land and ocean surfaces respectively are

$$0 = \Delta Q - \lambda_l \Delta T_l + f\Delta H_a, \tag{3}$$

$$\Delta H_o = \Delta Q - \lambda_o \Delta T_o - (1-f)\Delta H_a. \tag{4}$$

where λ_l and λ_o (both W m^{-2} K^{-1}) are the climate sensitivities over land and ocean respectively.

Depth dependent ocean temperature anomalies, $\Delta T_{o,s}(z,t) : z \geq 0$ (K) are modelled as satisfying the heat conduction equation

$$c_p \frac{\partial \Delta T_{o,s}}{\partial t} = \kappa \frac{\partial^2 \Delta T_{o,s}}{\partial z^2} \tag{5}$$

where $c_p = 4.04 \times 10^6$ (J K^{-1} m^{-3}) is the volumetric heat capacity of sea water, κ (W m^{-1} K^{-1}) is an effective thermal diffusivity, z (m) is depth into the ocean (positive downwards) and by definition, $\Delta T_{o,s}(0,t) = \Delta T_o(t)$. The ocean surface boundary condition is given by $\Delta H_o(t) = -\kappa \partial \Delta T_{o,s}/\partial z$ at $z = 0$ and by $\Delta T_{o,s} \equiv 0$ as $z \to \infty$ (here set as $z = 5000$m). Thermal advection is initially modelled as linear in land-ocean temperature anomaly contrast. That is

$$\Delta H_a = k(\Delta T_o - \Delta T_l) \tag{6}$$

where k (W m^{-2} K^{-1}) is an energy exchange coefficient (see for example Murphy (1995) and Rowntree (1998)).

GCM diagnostics are used to calibrate the two-box model parameters. As the land has no thermal capacity, the incoming advective flux anomaly must equal the top of the atmosphere radiation flux anomaly over land: $f\Delta H_a = -\Delta F_{TOA\downarrow,l}$. Combined with Eqs. (3) and (6) this allows λ_l and k to be diagnosed:

$$\lambda_l = \frac{\Delta Q - \Delta F_{TOA\downarrow,l}}{\Delta T_l}, \qquad k = \frac{-\Delta F_{TOA\downarrow,l}}{f(\Delta T_o - \Delta T_l)}. \tag{7}$$

Over the oceans a change in net downward top of the atmosphere radiative flux must balance anomalies in both the ocean heat flux and the advective flux to the land region: $\Delta F_{TOA\downarrow,o} = \Delta H_o + (1-f)\Delta H_a$. This condition combined with Eq. (4) and also noting that the only heat store for the entire system is the oceans yields

$$\lambda_o = \frac{\Delta Q - \Delta F_{TOA\downarrow,o}}{\Delta T_o}, \qquad \Delta H_o = \frac{\Delta F_{TOA\downarrow}}{f}. \tag{8}$$

The second equation provides an upper boundary condition to Eq. (5).

Diagnostics $\Delta T_l, \Delta T_o$, $F_{TOA\downarrow,l}$ and $F_{TOA\downarrow,o}$ (see Figures 2 a),b),d),e) respectively) from the 2% and 4x GCM experiments are used within Eqs. (7) and (8) to calculate decadal values of λ_l, λ_o and k (see Figures 2 c), f) and g)). The climate sensitivities are moderately well defined, i.e. near constant in time, especially λ_l. (Note, the parameters tend to be ill-defined for early decades when the GCM is near equilibrium and interdecadal variability can swamp the small climate change signal.) Parameter k is however, not robust and exhibits a wide range of values throughout the GCM model run. Figure 2 h) is a plot of $\Delta T_l/\Delta T_o$, which is a relatively conservative quantity. This observation is adopted as a surrogate constraint, expressed as

$$\Delta T_l = \nu \Delta T_o \tag{9}$$

that (implicitly) replaces the description of ΔH_a through parameter k. No physical explanation is offered here as to the processes leading to the robustness of parameter ν. However, this does seem to be a GCM diagnostic worthy of further investigation.

Based upon visual inspection of Figures 2 c), f) and h), values of $\lambda_l = 0.52$ (W m^{-2} K^{-1}), $\lambda_o = 1.75$ (W m^{-2} K^{-1}) and $\nu = \Delta T_l/\Delta T_o = 1.87$ are designated. The ocean heat diffusion model (5) is also solved, driven by surface heat flux $\Delta F_{TOA\downarrow}/f$. This is carried out by using an implicit numerical scheme with a sub-decadal timestep and for a range of different values of κ. With $\kappa = 384$ W m^{-1} K^{-1}, predictions of ΔT_o are almost indistinguishable from the full GCM values (see dotted line, Figure 2 d)) and so this value is adopted. The ocean surface temperature and surface heat flux may be related through an effective time dependent thermal heat capacity, $c^*_{p,o}(t)$ (as defined in Section 2.3.1) satisfying $c^*_{p,o}\mathrm{d}\Delta T_o/\mathrm{d}t = H_o$. An equivalent mixed-layer depth, $z_d(t)$ (m) satisfying $z_d = c^*_{p,o}/c_p$, is presented in Figure 2i). The behaviour of z_d is similar to that given by Keen and Murphy (1997), also for the 2% run.

The internal parameters of the two-box thermal model have now been evaluated and so the governing equations may be combined to give the complete model form. Eliminating H_a within Eqs. (3) and (4), and employing relationship (9) gives a surface boundary condition for Eq. (5) as

$$-\kappa \frac{\partial \Delta T_o}{\partial z} = \Delta H_o = \frac{\Delta Q(t)}{f} - \Delta T_o \left[\frac{(1-f)\lambda_l \nu}{f} + \lambda_o \right]. \tag{10}$$

Values of change in radiative forcing, ΔQ, are now the only input required by the two-box heat balance model. Eq. (5) with boundary condition (10) are used to calculate ΔT_o, from which ΔT_l may be evaluated using Eq. (9). Predicted surface temperature values are plotted in Figure 3 for all three profiles of ΔQ described in Section 2.2; also plotted are the mean decadal temperature anomaly values found directly from the three GCM transient runs. Figure 3 indicates that, in general, the two-box

model performs well although there is a tendency for the model to reach equilibrium temperatures too quickly for the 4x case. Model parameters have been selected through analysis of the 2% and 4x GCM run output only. The good fit to the GHG GCM run, representing a different forcing scenario, is a test of the two-box heat balance model when operated in a completely predictive fashion.

2.4 Calculation of the spatial patterns, $V_x(j,k)$

Patterns V_x are derived for each variable, spatial position and month, by direct calibration against anomalies as predicted by both the 2% and GHG GCM transient runs (thereby leading to two sets of patterns). For each variable V, for each month j, and for each spatial point k, $V_x(j,k)$ is found such as to minimise

$$I_V(j,k) = \sum_{i=1}^{N} [\Delta V(i,j,k) - \Delta T_l(i)\, V_x(j,k)]^2 \tag{11}$$

Values of $\Delta T_l(i)$ within Eq. (11) are calculated directly from the GCM anomalies (as opposed to the two box heat balance model), thereby decoupling the derived patterns from the model of global land temperature anomaly. Maps of $V_x(j,k)$ are presented for four months (January, April, July and September) for 1.5 m temperature (Figure 4) and rainfall (Figure 5).

3 The performance of the analogue model

3.1 General overview of the anomaly properties

Two statistics are calculated for each decade and for each set of anomalies as derived by the GCM transient run with GHG scenario forcings. For each variable V, and across all land points and months, the mean decadal anomaly value $\Delta V_\mu(i)$ and standard deviations ΔV_σ of the anomalies are calculated viz:

$$\Delta V_\mu(i) = \frac{\sum_{j=1}^{12}\sum_{k=1}^{1631} \delta A(k)\, \Delta V(i,j,k)}{12\,A}, \qquad \Delta V_\sigma(i) = \sqrt{\frac{\sum_{j=1}^{12}\sum_{k=1}^{1631} \delta A(k)\, [\Delta V(i,j,k) - \Delta V_\mu(i)]^2}{12\,A}}, \tag{12}$$

where $\delta A(k)$ (m^2) are model gridbox areas and A (m^2) is the total (gridbox) land surface area. These statistics are presented in Figure 6. For both temperature and downward longwave radiation, the mean anomaly values become larger than their decadal standard deviations, indicating a strong signal to noise variation as atmospheric greenhouse gases increase. A comparatively strong signal is also seen for relative humidity and snowfall. The overall significance of the anomaly variations can be measured by comparison with the mean values for each variable. Such values, appropriate to an observational climatology (A.D. Friend, personal communication), are listed in the plot titles or caption of Figure 6.

For the first few decades of the GHG GCM run, the radiative forcing is very small (see Figure 1) and as such initial values of ΔV_σ are representative of 'natural' interdecadal variability; the analogue model is not designed to explain these shorter timescale variations. However, all the standard deviations increase for later decades as the climate changes. This is consistent with the emergence of distinct spatial and seasonal anomaly patterns over and beyond a simple global linear shift. Under the assumptions contained within Eq. (1), this corresponds to variations within each array $V_x(j,k)$.

3.2 Analogue model performance for 1.5 m temperature

An initial assessment of the analogue model is undertaken by analysing its ability to reproduce GCM derived anomalies of 1.5m temperature, $\Delta T(i,j,k)$. Anomaly prediction by Eq. (1) is appraised for both the GHG and 2% forcing scenarios, with appropriate forcings supplied to the two-box heat balance model to derive $\Delta T_l(i)$. Consideration is given to the transferability of the patterns; for instance, can values of V_x derived from the 2% GCM run be used to predict GHG GCM run anomalies? A fundamental requirement is that the patterns are robust between different radiative forcing scenarios, thereby allowing the analogue model to be used predictively. The transferability between different forcings of the heat balance sub-model to estimate ΔT_l has already been considered in Section 2.3.2.

Analogue model skill is quantified for variable V by its decadal root mean square error ϵ_V when predicting GCM anomalies. Calculated across all months and spatial positions, this statistic is given

by

$$\epsilon_V(i) = \sqrt{\frac{\sum_{j=1}^{12}\sum_{k=1}^{1631}\delta A(k)[\Delta V(i,j,k) - \Delta T_l(i)V_x(j,k)]^2}{12A}}. \quad (13)$$

This statistic for 1.5m temperature, $\epsilon_T(i)$ (K) is presented in Figure 7a) for the GHG radiative forcing profile. This corresponds to using patterns T_x derived from the GHG GCM run (continuous line) and the 2% GCM run (dashed line). Throughout all decades, there is no overall increase in ϵ_T for increasing decades i and when using patterns from the GHG GCM run. Hence the analogue model performs very well in capturing all extra variation (over inter-decadal variability) for this case; here the assumption of separability implicit within the analogue model appears valid. The increase in ϵ_T for later decades and when using patterns from the 2% run indicates some degradation in analogue model performance. This is a consequence of interchanging patterns from the strongly forced 2% run; the importance of such reduction in performance when compared to mean anomaly behaviour can be assessed by observation of the first plot of Figure 6.

In Figure 7 b), the analogue model's ability to predict 2% GCM diagnostics of temperature is shown using patterns derived from the 2% GCM run (continuous line) and from the GHG GCM run (dashed line). The continuous line again shows good performance when patterns associated with a particular radiative forcing scenario (here the 2% run) are used to rederive anomalies for the same forcing scenario. However, there is some evidence of a mid-run reduction in skill (around the decade starting 1910) and this is attributed to the large changes in forcing encountered during the 2% run, causing a partial breakdown of the assumption of linearity contained within Eq. (1). If for each spatial position and month, curvature occurs within plots of local temperature anomalies $\Delta T(i,j,k)$ against global mean temperature anomaly, $\Delta T_l(i)$, the linear fitting procedure (leading to values of $T_x(j,k)$) may produce the largest errors towards the middle of the intercomparison period.

There are two distinct features associated with the dashed curve in Figure 7 b). For decades before 1920, the use of patterns found through comparison with the GHG run actually perform better than those found directly from the 2% GCM run. Figure 1 shows that up to 1920, the 2% run experiences the same range of extra radiative forcing as the full GHG run ($\Delta Q = 6.31$ W m^{-2} at the end of the GHG run and $\Delta Q = 6.41$ W m^{-2} in year 1920 for the 2% run). Similarly, from Figure 3, the mean value of ΔT_l during the last decade of the GHG run is nearly identical to that during the decade ending 1930 for the 2% run (5.60 K and 5.67 K respectively). The second feature is that using the patterns derived from the GHG GCM run to predict anomalies towards the end of the 2% run results in a large degradation of analogue model performance. The implication is that the analogue model performs well provided the range of radiative forcing prescribed to the model does not exceed that used in the original pattern calibration exercise.

In summary, for 1.5m temperature and using patterns derived from the GHG GCM run, the analogue model performs well in reproducing anomalies from the GHG GCM run. More importantly, the analogue model (again using patterns from the GHG GCM run) performs very well in predicting anomalies during the early stages of the 2% GCM run when a similar range of radiative forcings to the GHG run are encountered. Performance deteriorates when extrapolating beyond the range of radiative forcings for which the analogue model has been calibrated. The analogue model with patterns derived against the more extreme 2% GCM run show some loss of predictive ability when used to estimate the GHG GCM anomalies, although they perform well overall when reproducing the 2% GCM anomalies. The assessment of analogue model performance is of particular consequence when using patterns calibrated against one GCM transient run to forecast anomalies from a second GCM run, for this represents model operation in a strictly predictive mode.

3.3 Analogue model performance for all variables

Identical analyses to those of Section 3.2 are undertaken for all the land surface variables. Values of ϵ_V are given in Figure 8 using the analogue model to predict GHG GCM anomalies with patterns derived from the GHG run (continuous lines) and the 2% run (dashed lines). Similarly in Figure 9, values of ϵ_V are shown corresponding to predictions of the 2% run with patterns derived from the 2% run (continuous lines) and the GHG run (dashed lines). In general, for all combinations of patterns and prescribed forcings, the quantitative behaviour of all anomaly variables closely follows that found for the 1.5 m temperature.

Also plotted, for comparison with ϵ_V values, are the decadal standard deviations of anomalies $\Delta V_\sigma(i)$ (see Eq. (12) and also Figure 6) and the root mean square anomaly values (relative to the control climate) given by

$$\Delta V_{TOT}(i) = \sqrt{\frac{\sum_{j=1}^{12} \sum_{k=1}^{1631} \delta A(k)[\Delta V(i,j,k)]^2}{12A}}. \tag{14}$$

As discussed in Section 3.1, statistic ΔV_σ demonstrates the importance of evolving seasonal and spatial patterns relative to mean anomaly change, whereas ΔV_{TOT} encapsulates total variability within anomalies, that is both developing patterns and any long-term trends. For some variables (eg windspeeds), it is observed that the statistics ΔV_σ and ΔV_{TOT} are nearly identical, indicating that there is very little change in the global mean anomaly, but spatial and seasonal patterns emerge.

A procedure is required that indexes analogue model performance for the different land surface climatological variables. As the quantitative deductions of Section 3.2 relating to the 1.5m temperature are found to be valid for all variables, then the development of a simple ordering statistic is possible. An appropriate test is to use 1) well-defined patterns within the analogue model for 2) a radiation forcing profile ΔQ that is different to the original calibration GCM run (thereby operating predictively) and 3) ensuring that there is not significant extrapolation beyond the climate regime experienced within the original pattern calibration exercise. For these reasons (and referring to the analysis of Section 3.2), the prediction of anomalies from the 2% GCM run during the initial decades and with patterns derived from the GHG GCM are selected for consideration. Based upon the seventh decade of the 2% run, (a decade beyond which ΔQ for the 2% run significantly exceeds that for the last decade of the GHG run) and with $\Delta V_{TOT}(1)$ assumed to estimate the interdecadal variability, ordering statistic S_V is given by

$$S_V = 100\left[1 - \left(\frac{\epsilon_V(7) - \Delta V_{TOT}(1)}{\Delta V_{TOT}(7) - \Delta V_{TOT}(1)}\right)\right]. \tag{15}$$

Values of S_V are presented in Table 1 and they broadly indicate the percentage of change in variable V over and beyond interdecadal variation (ie $\Delta V_{TOT}(7) - \Delta V_{TOT}(1)$) that the analogue model is capable of explaining. The analogue model is particularly good at predicting changes in 1.5 m temperature and downward longwave radiation; this may be expected as these variables contain large "signal to noise" ratios (see Figure 6). Other variables for which the analogue model performs well are 1.5m relative humidity and windspeeds. The analogue model is weakest at predicting transient GCM anomalies in rainfall rate. The statistic for snowfall rate appears to be good, although there are large regions where snowfall will be consistently zero. In areas where the GCM predicts snowfall, the analogue model may not perform as well as suggested by Table 1.

Variable	ΔT	Δr_h	Δu	Δv	$\Delta R_{L,\downarrow}$	$\Delta R_{S,\downarrow}$	ΔP_R	ΔP_S	Δp_0
$S_V(\%)$	96	82	80	81	96	79	68	94	76

Table 1: Statistic S_V calculated for 1.5m temperature (ΔT), 1.5m relative humidity (Δr_h), 10.0m zonal windspeed (Δu), 10.0m azimuthal windspeed (Δv), downward longwave radiation ($\Delta R_{L,\downarrow}$), downward total shortwave radiation ($\Delta R_{S,\downarrow}$), rainfall rate (ΔP_R), snowfall rate (ΔP_S)and surface pressure anomalies (Δp_0)

3.4 An example application - changes in terrestrial carbon storage

The analogue model is used to provide driving conditions for a large scale dynamic terrestrial carbon cycle model, "TRIFFID", designed for implementation within a GCM. Key features of this ecosystem model are that it calculates biosphere diagnostics of soil and vegetation carbon, themselves a function of the predicted structure and coverage of (five) plant functional types. The areal coverage, leaf area index and canopy height are updated based upon carbon fluxes calculated within a coupled canopy conductance and photosynthesis module, which is sensitive to both the land surface climatology and the CO_2 concentration (Cox et al. (1998)). TRIFFID is a dynamic model, which explicitly allows for vegetation growth, death and competition within a changing climate, and as such may demonstrate important temporal effects that would be undetected by equilibrium vegetation models.

TRIFFID is "spun up" to equilibrium using an observational climatology (Friend, personnal communication) and the CO_2 concentration assumed at the beginning of each of the GCM runs (290 ppmv for the 2% run and 286.3 for the GHG run). For each GCM scenario, dynamical TRIFFID simulations are carried out using both the anomalies directly from the GCM and also the anomalies calculated by the analogue model. In the latter case, patterns derived from the GHG GCM run are used for both forcing scenarios, for the reasons given in Sections 3.2 and 3.3. Although TRIFFID calculates many diagnostics, in this test study only the change in terrestrial (vegetation plus soil) carbon storage anomaly, ΔC_T (kg C m^{-2}) is analyzed.

In Figure 10, values of ΔC_T are plotted for a) the GHG scenario and b) the 2% scenario with anomalies derived directly from the GCM (continuous lines) and from the analogue model (dashed lines). Also plotted (dotted lines) are the root mean square errors, ϵ_{C_T} (kg C m^{-2}), of the analogue model when predicting GCM anomalies (see Eq. (13) for statistic definition and where variable V is terrestrial carbon storage). There is a very close relation between predictions of changes in terrestrial carbon storage for both GCM anomalies and the analogue model. For information, the critical point observed within Figure 10 b) is broadly due to CO_2 fertilisation of photosynthesis becoming superceeded by temperature enhanced respiration at later decades.

As the terrestrial carbon cycle model is dynamic (and thereby contains both an "inertia" and "memory"), discrepancies between the GCM and analogue model predictions of anomalies in driving climatological data will result in a gradual increase in ϵ_{C_T}. This may be observed for the initial decades in Figures 10 a) and b). However, throughout the rest of the GHG run and up to approximately year 1930 of the 2% run, ϵ_{C_T} is quite conservative. This suggests that errors in prediction of C_T when driven by anomalies from the analogue model rather than GCM derived anomalies is due to interdecadal variability only. This may be expected from the preceding direct analysis of driving variables for the identical time-periods (see Sections 3.2 and 3.3). That is, with no evolving long term differences between GCM and analogue model derived driving data anomalies, it may be anticipated that model predictions of C_T would also be similar. It is noted that for the later years of the 2% run, although predictions of the absolute values of C_T are similar, the root mean square error increases, implying that the pattern of terrestrial carbon storage change is not well reproduced when extrapolating to such extreme conditions.

To provide additional verification that the analogue model is an effective tool to predict ΔC_T, maps are produced of ΔC_T for the last year of the GHG run (Figure 11) and year 1930 of the 2% run (Figure 12). The predicted pre-industrial terrestrial carbon contents C_T are shown for comparison (maps a)). Changes in terrestrial carbon storage are plotted for TRIFFID driven by the GCM anomalies directly (maps b)) and driven by the analogue model (maps c)). Distinct spatial patterns emerge in anomalies ΔC_T, but the difference between using GCM and analogue model derived surface climatology forcings is minimal (compare individual maps b) to maps c)). Of particular interest, however, is that there are some differences between Figures 11 c) and 12 c). As discussed in Section 3.2, the analogue model land surface climatologies provided to the terrestrial carbon cycle model during the decade ending 2100 for the GHG run will nearly correspond to those for the decade ending 1930 in the 2% run. Associated differences in ΔC_T are therefore a consequence of the interactions between the implicit timescales of the dynamic terrestrial carbon cycle model, and those associated with the prescribed atmospheric forcings. They are also a consequence of differing values of atmospheric CO_2 influencing the photosynthetic model at these times (some of the GHG run atmospheric forcing is due to other greenhouse gases).

The power of the analogue modelling approach is that differing terrestrial responses can be quickly investigated for a range of imposed forcing scenarios without recourse to a completely new GCM transient run. This means an ecosystem phenomenon found when using anomalies from a GCM transient run can be tested for robustness across a range of other forcing scenarios. Future analogue model developments may include relating changes in terrestrial biomass to perturbations in prescribed atmospheric CO_2 concentration and surface-climate feedbacks. A simple ocean CO_2 uptake model could also be included to create a complete "off-line" global carbon cycle model (Joos et al. (1996)) which would include zeroth order climate feedbacks.

4 Conclusions

The analogue model generates decadal anomalies in land surface climatology as classified by the particular variable of interest, land spatial position and month. The model contains two distinct features. The decadal global mean land surface temperature anomaly, ΔT_l, is related to changes in atmospheric radiative forcing by a simple land-ocean heat balance model and with internal parameters derived from GCM transient run diagnostics. The second component is a set of spatial patterns V_x for each month and each variable which represent linearities between the anomalies and ΔT_l; these are found by calibration against GCM output. The existence of such linearity has been confirmed within GCM derived anomalies corresponding to a transient run with radiative forcings appropriate to anthropogenic emissions between the pre-industrial period and now, followed by the IPCC IS92a scenario (the "GHG" run). To a slightly lesser degree, such linearity exists within GCM diagnostics corresponding a more extreme fourteen decade transient experiment representing a cumulative increase by two percent per annum of atmospheric carbon dioxide (the "2%" run).

Analysis shows that the two-box heat balance model for ΔT_l is robust inasmuch as it performs well for different profiles of radiative forcing but with the same internal parameters. Similarly, patterns V_x are transferable between different forcing scenarios when the range of new forcings encountered do not exceed those experienced within the original calibration of patterns against GCM output. This is the case whereby the analogue model with patterns V_x tuned against the GHG run is found to accurately predict anomalies for the first seven decades of the 2% GCM run.

Parameters within the two-box heat balance model for ΔT_l and the patterns V_x retain much information about the temporal and spatial behaviour of existing GCM experiments. Subject to the proviso of not extrapolating greatly beyond the original range of climate change used to calibrate V_x, the analogue model provides a very efficient methodology for generating decadal mean anomalies. The anticipated use is to generate surface climatological anomalies as required by impact studies and for scenarios of radiative forcings for which full GCM transient experiments do not currently exist.

5 Acknowledgements

This work was supported by a subcontract with the Hadley Centre and NERC Science Budget funds (Chris Huntingford) and by the UK DETR Climate Prediction Programme under contract PECD 7/12/37 (Peter Cox). The authors thank William Ingram for his forcing data appropriate to the GHG run and Chris Taylor, John Gash and Richard Harding for their valuable suggestions on an early draft of this paper.

References

Cox PM, Huntingford C, Harding RJ (1998) A canopy conductance and photosynthesis model for use in a GCM land surface scheme. Journal of Hydrology 212–213:79–94.

Cox PM, Betts RA, Bunton CB, Essery RLH, Rowntree PR, Smith J (1999) The impact of new land surface physics on the GCM sensitivity of climate and climate sensitivity. Climate Dynamics 15:183–203.

Edwards J, Slingo A (1996) Studies with a flexible new radiation code. I: Choosing a configuration for a large-scale model. Quarterly Journal of the Royal Meteorological Society 122:689–720.

Gordon C, Cooper C, Senior C, Banks H, Gregory J, Johns T, Mitchell J, Wood R (1998) The simulation of SST, sea ice extents and ocean heat transport in a version of the Hadley Centre coupled model without flux adjustments. Climate Dynamics Submitted.

Joos F, Bruno M, Fink R, Siegenthaler U, Stocker T, Quere CL, Sarmiento J (1996) An efficient and accurate representation of complex oceanic and biospheric models of anthropogenic carbon uptake. Tellus 48B:397–417.

Keen AB, Murphy JM (1997) Influence of natural variability and the cold start problem on the simulated transient response to increasing CO_2. Clim Dyn 13:847–864.

Kershaw R, Gregory D (1997) Parametrization of momentum transport by convection. Part I. Theory and cloud modelling results. Quarterly Journal of the Royal Meteorological Society 123(541):1133–1151.

Mitchell J, Johns T, Eagles M, Davies R (1998) Towards the construction of climate change scenarios. Climatic Research Submitted.

Murphy JM (1995) Transient response of the Hadley Centre coupled ocean-atmosphere model to increasing carbon dioxide: Part III. Analysis of global-mean response using simple models. J Climate 8:496–514.

Pope VD, Gallani ML, Rowntree PR, Stratton RA (Submitted) The impact of new physical parametrizations in the Hadley Centre Climate Model - HadAM3. Climate Dynamics.

Rowntree P (1998) Global average climate forcing and temperature response since 1750. International Journal of Climatology 18:355–377.

Shine K, Derwent R, Wuebbles D, Morcrette JJ (1990) Radiative forcing of climate. In: Houghton J, Jenkins G, and Ephraums J (eds), Climate Change. The IPCC scientific assessment chapter 5, 45–68. Cambridge University Press Cambridge.

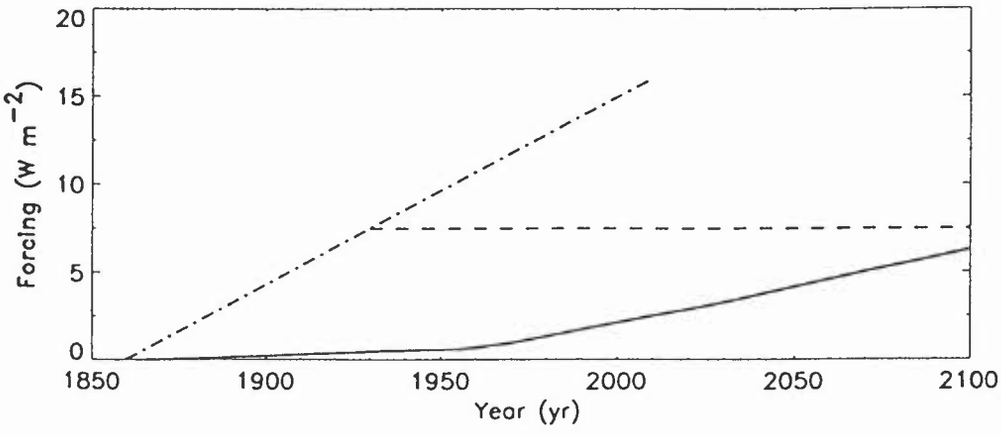

Figure 1: The forcing anomalies applicable to the GHG (continuous line), 2% (dash-dot line) and 4x (dashed line) GCM experiments.

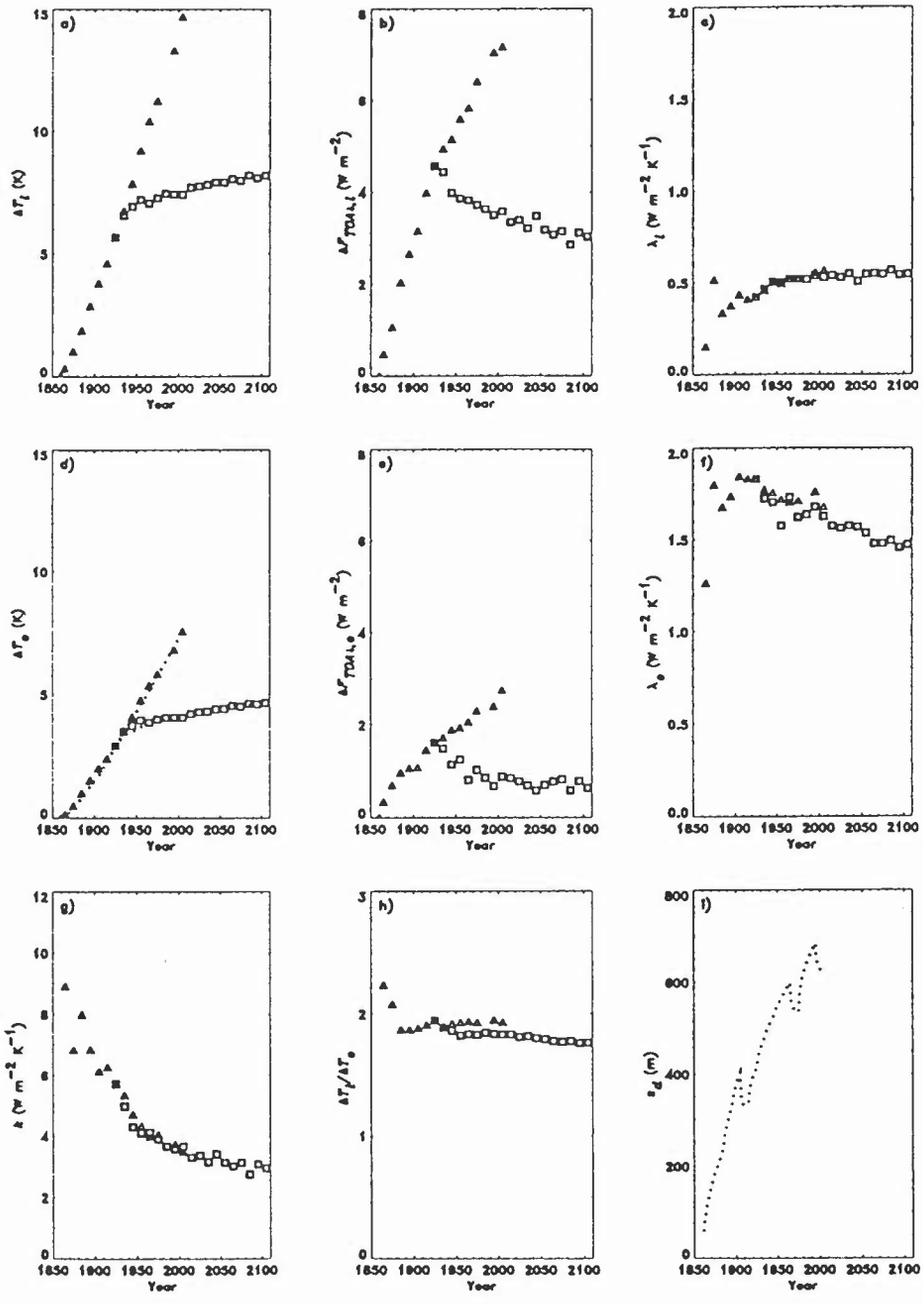

Figure 2: Mean decadal GCM diagnostics (for the 2% (□)and 4x (△) runs) of a) ΔT_l, b) $\Delta F_{TOA\downarrow,l}$, d) ΔT_o, e) $\Delta F_{TOA\downarrow,o}$ and h) $\Delta T_l/\Delta T_o$. Also plotted are inferred values of c) λ_l, f) λ_o and g) k (see Section 2.3.2). The ocean heat diffusion model (with κ = 230 W m^{-1} K^{-1} and surface forcing $F_{TOA\downarrow}$: see Section 2.3.2) estimates d) ΔT_o (dotted line) and equivalent mixed-layer depth i) z_d. All variables are as a function of (model) year.

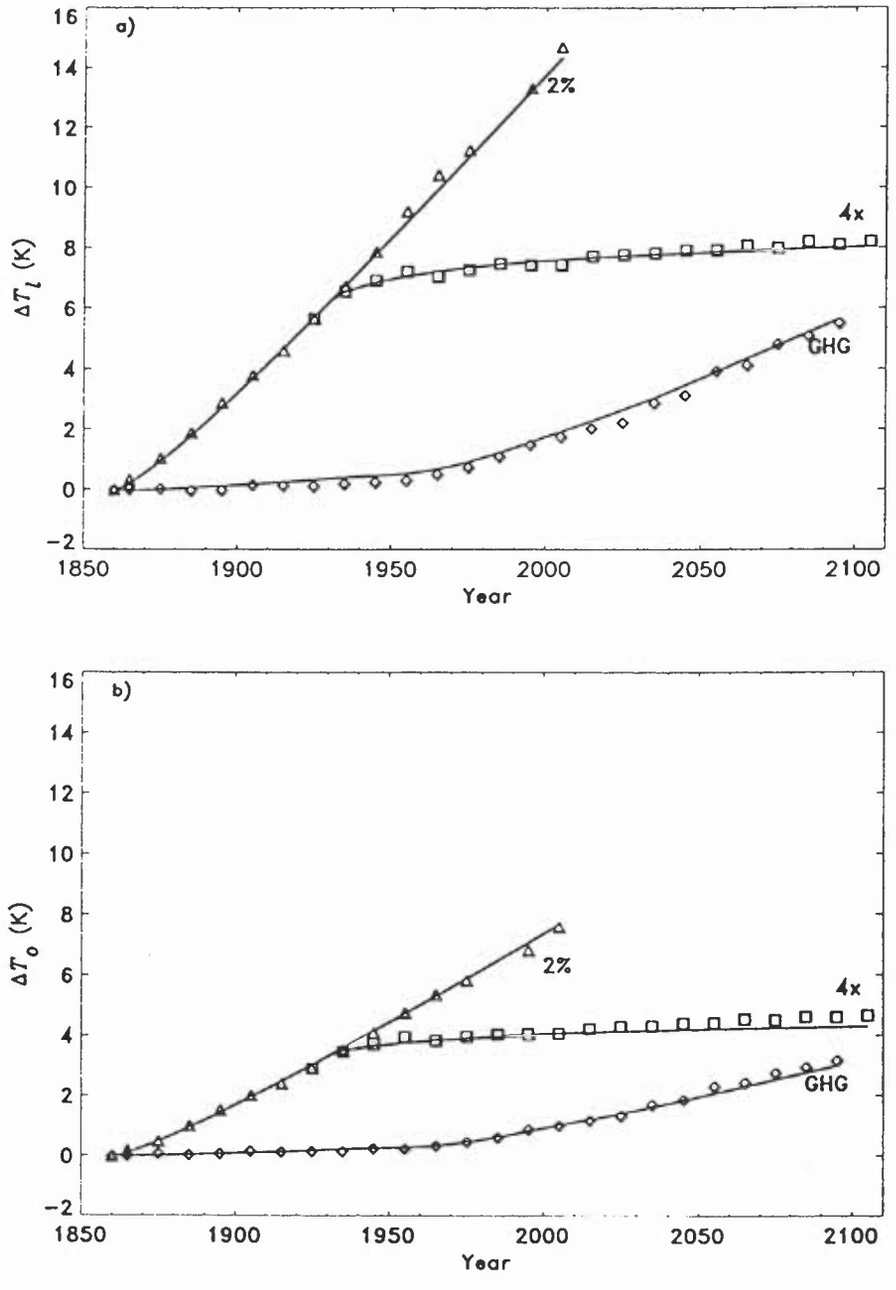

Figure 3: Two-box model predictions (continuous lines) of a) decadal mean land surface temperature and b) decadal mean ocean surface temperature, for radiative forcing scenarios appropriate to the 2%, 4x and GHG scenarios. Also plotted, for comparison, are the actual GCM decadal mean anomaly values for the (□) 2%, (△) 4x and (◇) GHG GCM runs. The values plotted for 1860 are representative of long-term averages from a "pre-industrial" control run.

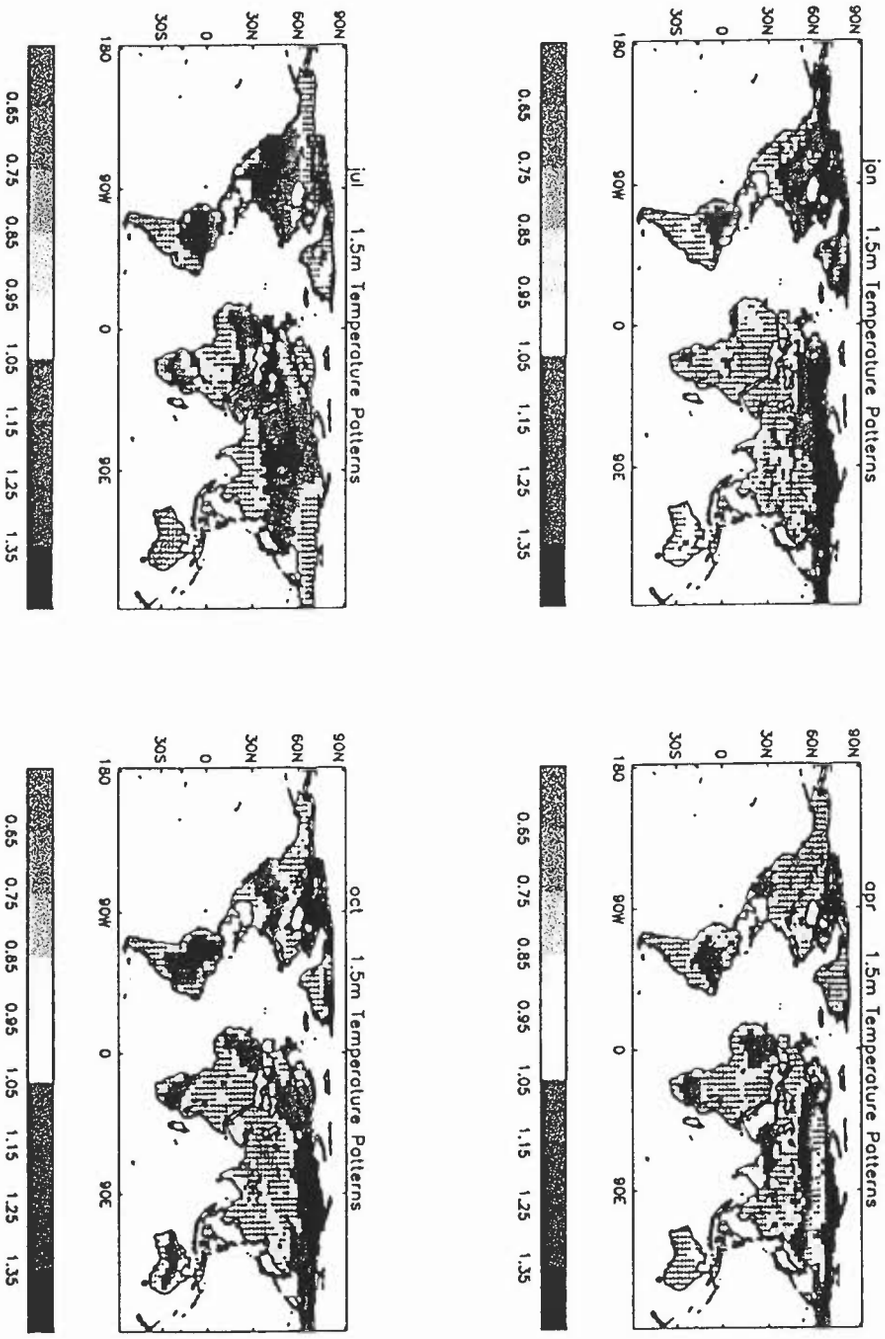

Figure 4: Patterns of 1.5 m temperature change, T_x, for the months of January, April, July and October. The heavy dots denote values below 0.95.

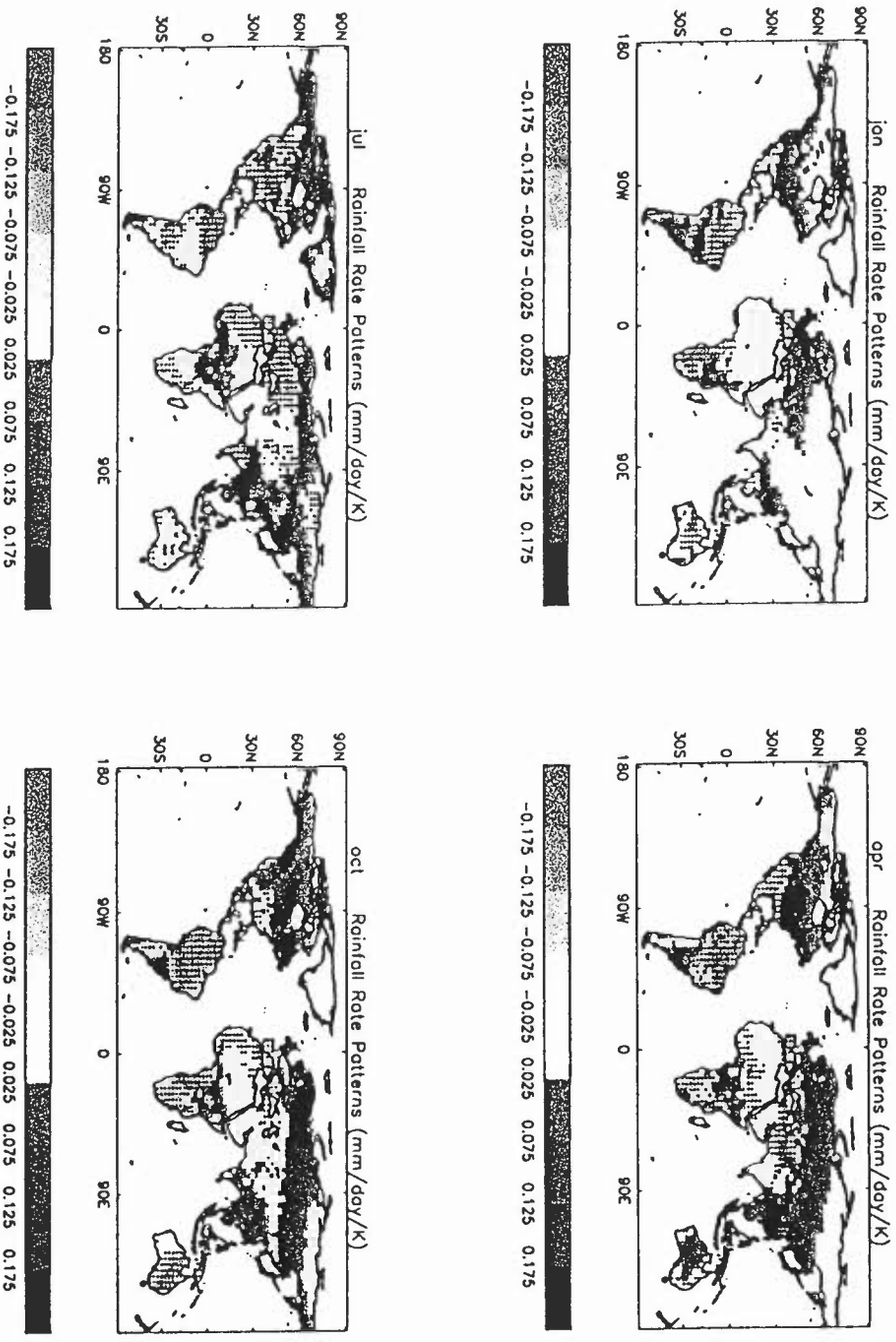

Figure 5: Patterns of rainfall change P_x (mm day^{-1} K^{-1}) for the months of January, April, July and October. The heavy dots denote values below -0.025 mm day^{-1} K^{-1}.

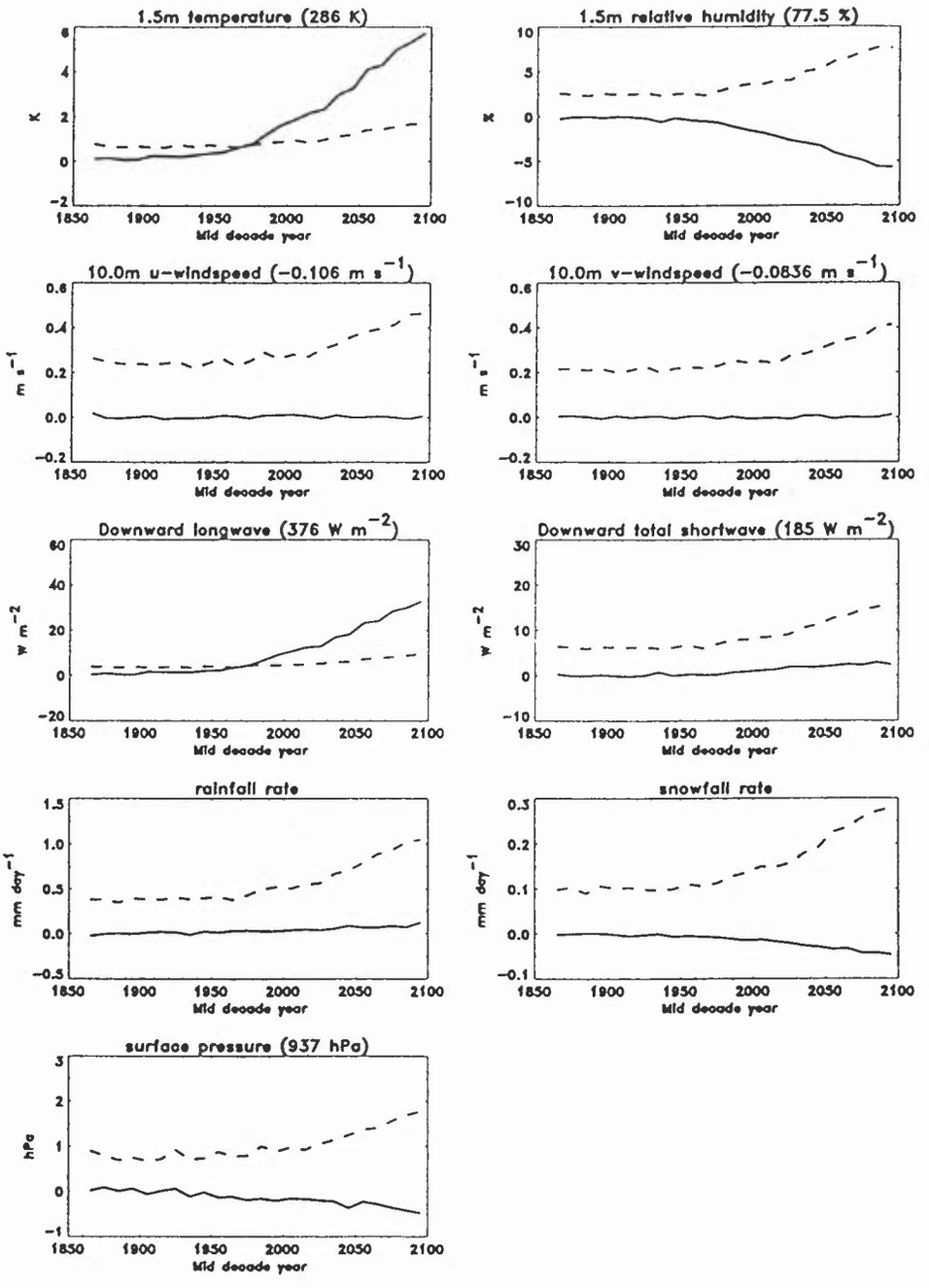

Figure 6: Decadal mean anomalies (continuous lines) and related standard deviations (dashed lines) across all land points and for all months as predicted by HadCM3 using the GHG forcings. Global mean values from the observational climatology are provided in brackets after the title. This climatology combines rainfall and snowfall rates, to give a global mean precipitation rate of 2.15 mm day^{-1}. The global mean value of windspeed, $\sqrt{u^2 + v^2}$, is 1.99 m s^{-1}.

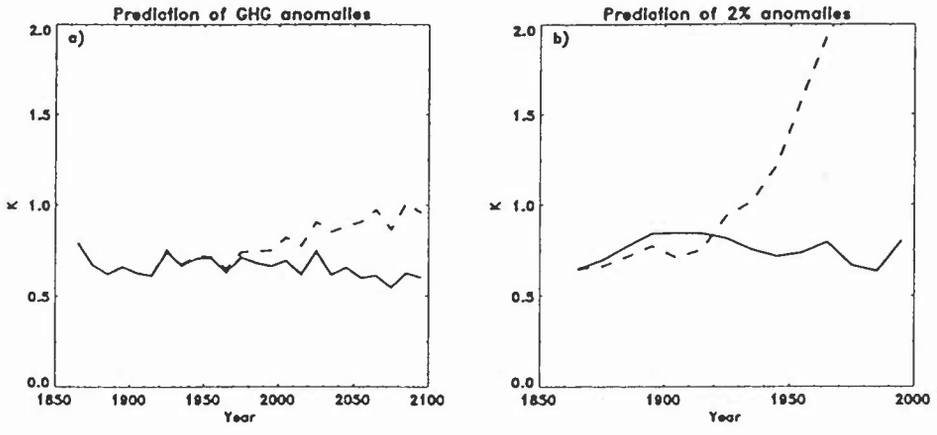

Figure 7: Values of $\epsilon_T(i)$ for each decade (mid-decade year plotted) corresponding to a) predictions of the GHG temperature anomalies by the analogue model using patterns derived from the GHG GCM run (continuous line) and the 2% GCM run (dashed line). Similarly, plot b) corresponds to predictions of the 2% anomalies by the analogue model using patterns derived from the 2% GCM run (continuous line) and the GHG GCM run (dashed line).

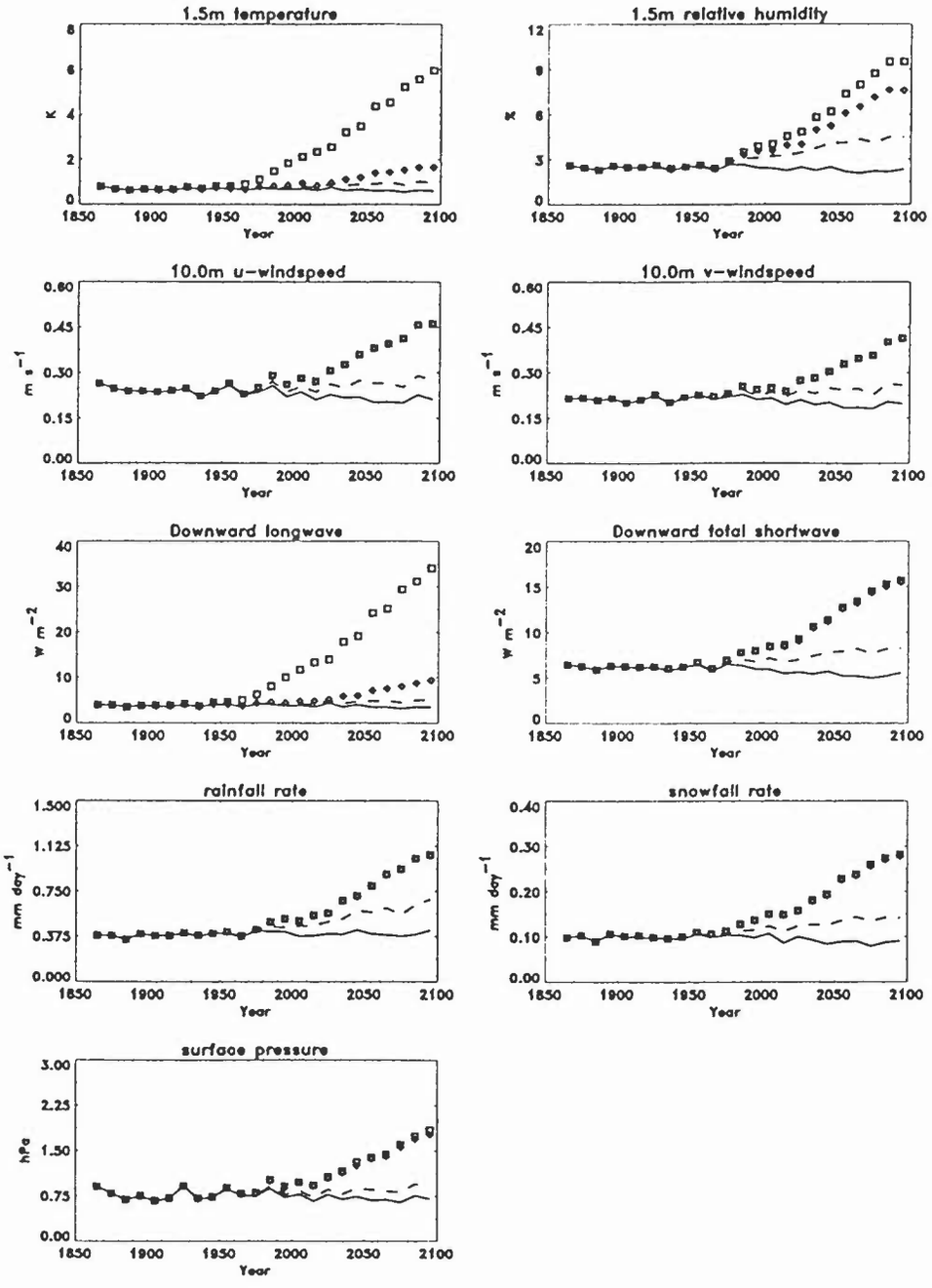

Figure 8: Values of ϵ_V for each decade corresponding to predictions of the GHG GCM anomalies by the analogue model for each variable V (see individual plot titles) and using patterns derived from the GHG run (continuous lines) and the 2% run (dashed lines). Statistics $\Delta V_a(i)$ ($\diamond$) and ΔV_{TOT} ($\square$) are also plotted.

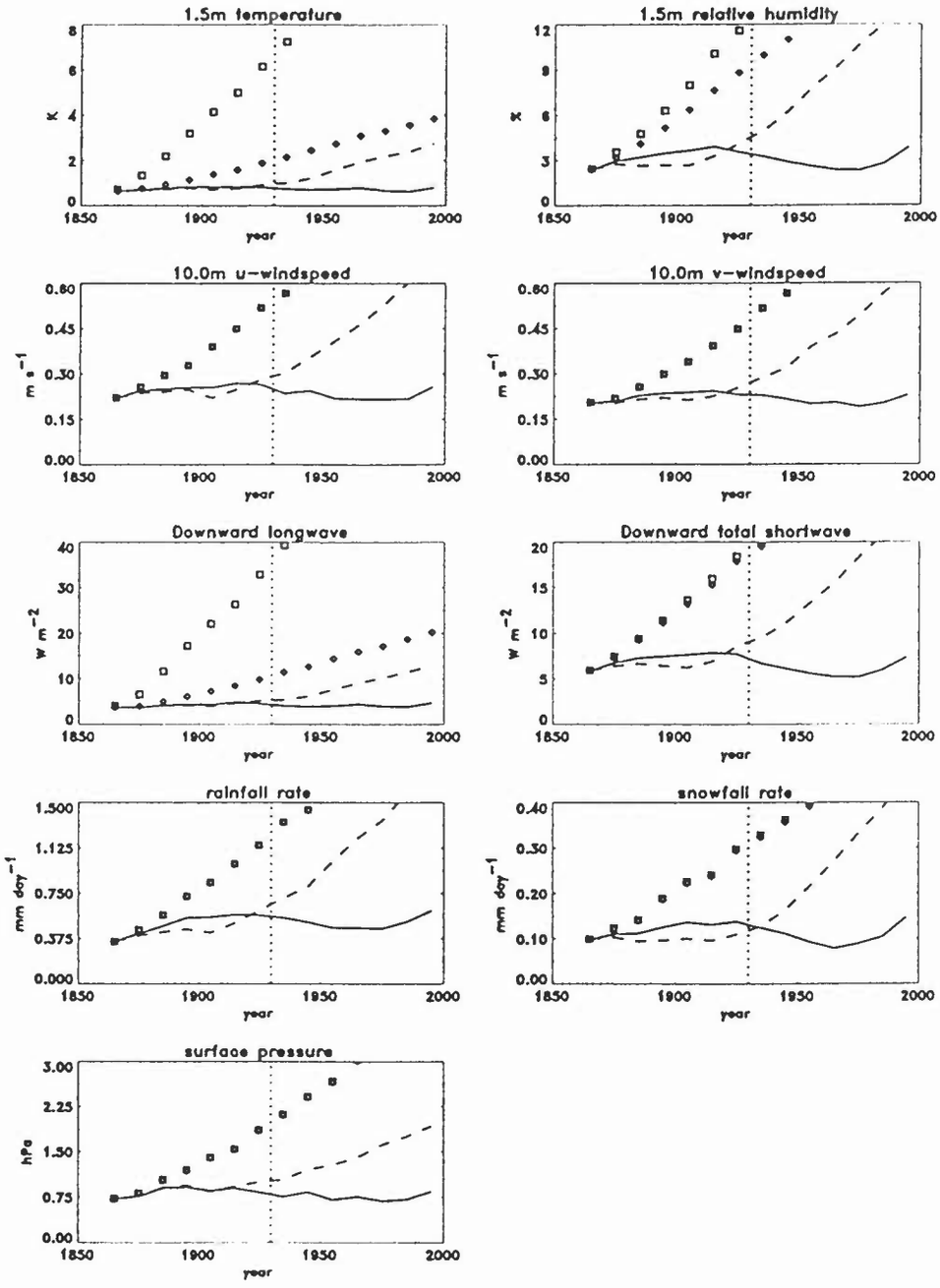

Figure 9: Values of ϵ_V for each decade corresponding to predictions of the 2% GCM anomalies by the analogue model for each variable V (see individual plot titles) and using patterns derived from the 2% run (continuous lines) and the GHG run (dashed lines). Statistics $\Delta V_a(i)$ ($\diamond$) and ΔV_{TOT} ($\square$) are also plotted. The dotted vertical line marks the end of the last decade during which ΔQ and T_l values for the 2% run are comparable to those encountered at some point within the GHG run.

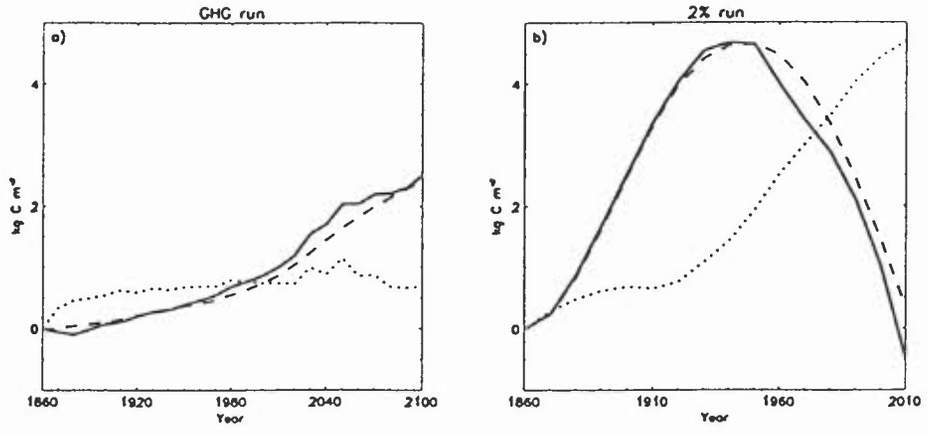

Figure 10: Changes in total terrestrial carbon, ΔC_T (kg C m^{-2}) as simulated by TRIFFID when forced by anomalies prescribed directly from the GCM (continuous line) and when forced by the analogue model (dashed line), for a) the GHG radiative forcing scenario and b) the 2% forcing scenario. The analogue model uses patterns derived against the GHG GCM run in both cases. Also plotted (dotted line) for both radiative forcings scenarios, ΔQ, are the root mean square errors calculated using statistic ϵ_V (Eq. 13) and applied to diagnostic ΔC_T.

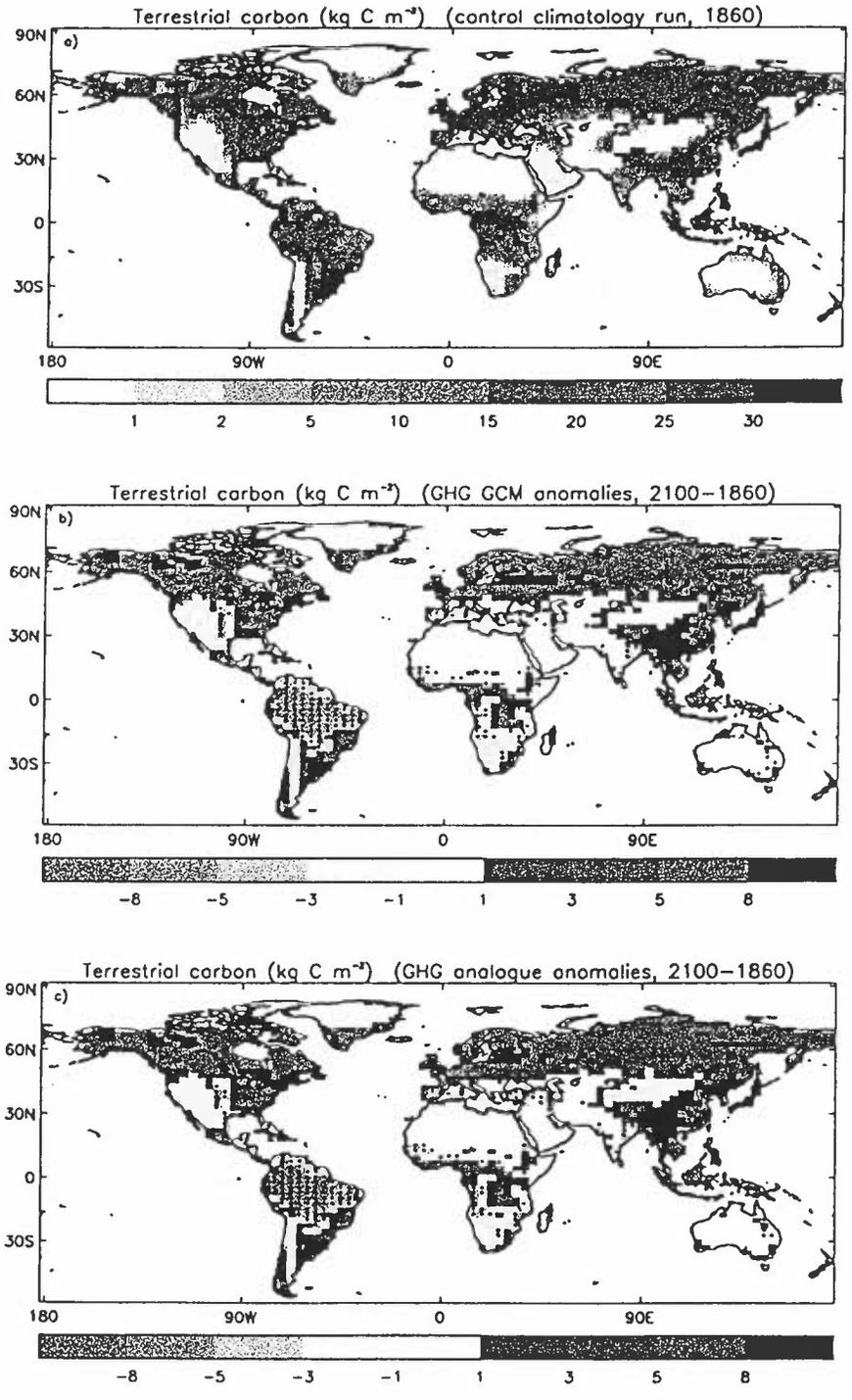

Figure 11: A map of a) equilibrium terrestrial carbon storage, C_T (kg m^{-2}) as simulated by TRIFFID for the observational climate, and changes in terrestrial carbon storage during the period of the simulations, ΔC_T (kg m^{-2}) (also as predicted by TRIFFID) when driven by b) GCM anomalies for the GHG run and c) the analogue model using patterns derived against the GHG GCM run. The heavy dots denote values below -1 kg m^{-2}.

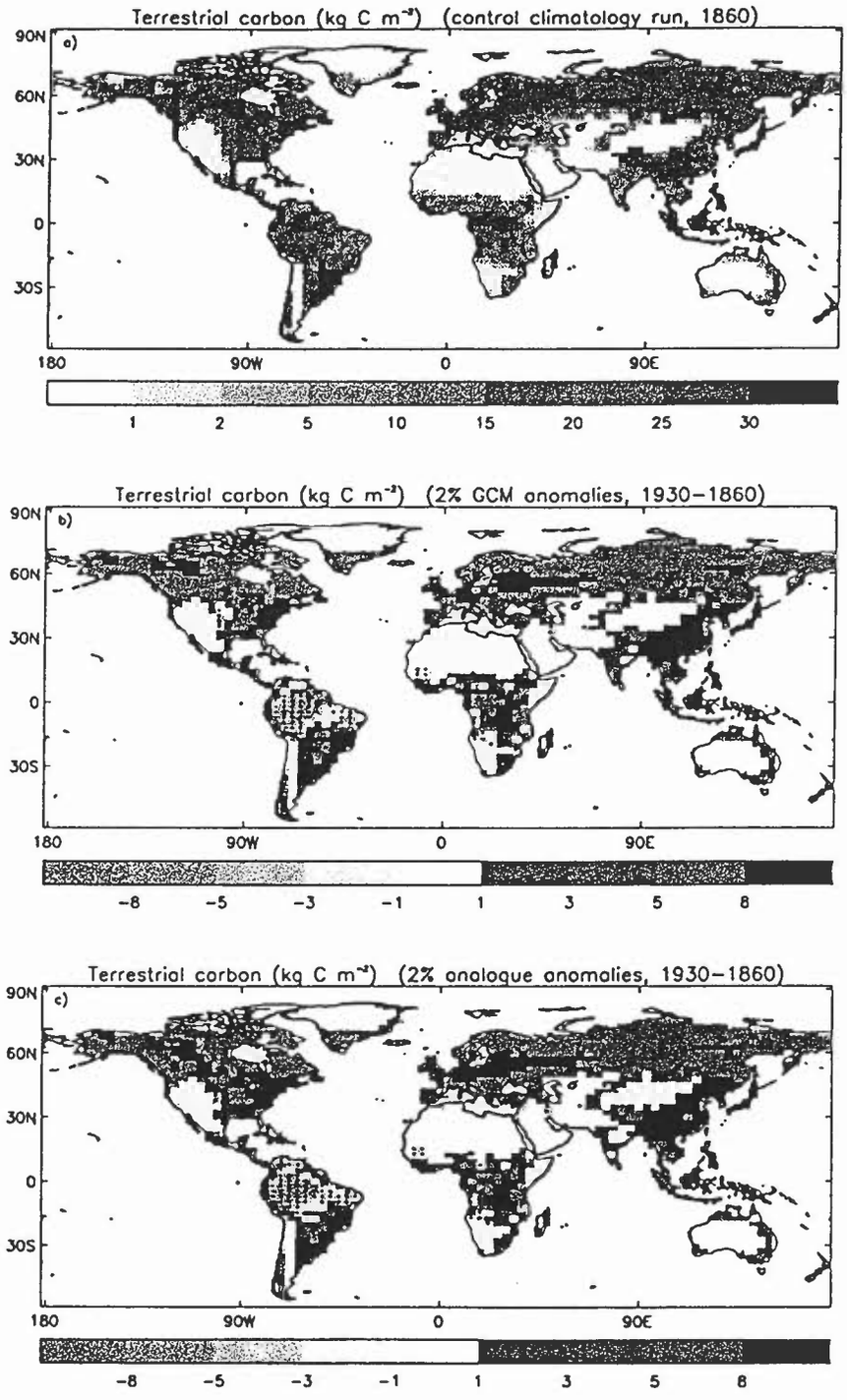

Figure 12: A map of a) equilibrium terrestrial carbon storage, C_T (kg m^{-2}) as simulated by TRIFFID for the observational climate, and changes in terrestrial carbon storage ΔC_T (kg m^{-2}) for 1930 (also as predicted by TRIFFID) when driven by b) GCM anomalies for the 2% run and c) the analogue model, using patterns derived against the GHG GCM run. The heavy dots denote values below -1 kg m^{-2}.